frontiers | Frontiers in Built Environment

TYPE Original Research
PUBLISHED 24 September 2025
DOI 10.3389/fbuil.2025.1620385

OPEN ACCESS

EDITED BY
Alberto Viskovic,
University of Studies G. d'Annunzio Chieti and Pescara, Italy

REVIEWED BY
Jairo José De Oliveira Andrade,
Pontifical Catholic University of Rio Grande do Sul, Brazil
Peng Zhang,
Zhengzhou University, China

*CORRESPONDENCE
Bahar Gharehpapagh,
bahar.gharehpapagh@imkf.tu-freiberg.de

RECEIVED 29 April 2025
ACCEPTED 29 August 2025
PUBLISHED 24 September 2025

CITATION
Denker M, Gharehpapagh B, Gruhn R, Pose S, Korniejenko K, Grab T and Zeidler H (2025) Compressive strength of geopolymer with recycled carbon fibres manufactured in air and in water by casting and additive manufacturing.
Front. Built Environ. 11:1620385.
doi: 10.3389/fbuil.2025.1620385

Compressive strength of geopolymer with recycled carbon fibres manufactured in air and in water by casting and additive manufacturing

Meike Denker[1], Bahar Gharehpapagh[1]*, Richard Gruhn[2], Sebastian Pose[2], Kinga Korniejenko[3], Thomas Grab[2] and Henning Zeidler[1]

[1]Institute for Machine Elements, Engineering Design and Manufacturing, Technische Universität Bergakademie Freiberg, Freiberg, Germany, [2]Scientific Diving Center of the Technische Universität Bergakademie Freiberg, Freiberg, Germany, [3]Faculty of Material Engineering and Physics, Cracow University of Technology, Cracow, Poland

Geopolymers (GPs) are inorganic binders synthesised from reactive aluminosilicate materials such as metakaolin, fly ash, and blast furnace slag, using strongly alkaline solutions at room temperature. They are more environmentally friendly than Portland cement and exhibit high hardness, weathering resistance, thermal stability, and precise mouldability. These properties make them suitable for additive manufacturing (AM) and specialised underwater applications, such as encapsulating hazardous substances or stabilising corroding shipwrecks. This study investigates the compressive strength of metakaolin-based GP reinforced with recycled carbon fibres, comparing performance in different water environments over time. Samples were produced by mould casting in air, manual underwater extrusion, and AM via material extrusion with chemical reaction bonding (MEX-CRB) in air. The 3D-printed and mould-cast samples produced in air were stored for up to 3 months in different water environments with varying salt and mineral contents to assess durability, mechanical performance, and environmental impact at defined intervals. For manually printed underwater specimens, the storage period was extended to almost 6 months, with only conducted in tap water conditions. Mould-cast specimens in air reached ~50 MPa, while MEX-CRB samples achieved ~20 MPa; after 3 months in salt water, mould-cast samples retained ~30 MPa, whereas printed ones remained below 20 MPa. Manually printed underwater samples increased from ~8 MPa at casting to ~14–15 MPa by week 4 before stabilizing. Microstructural observations showed crack-bridging by fibres, with random orientation in cast samples improving isotropic strength, while fibre alignment and higher porosity in printed samples limited performance. The water analysis results underscore the environmentally friendly potential of GPs in reducing environmental risks

and developing sustainable methods for underwater construction and hazard prevention.

KEYWORDS

geopolymer, additive manufacturing, material extrusion, compressive strength, underwater applications, long-term investigations

1 Introduction

Additive Manufacturing (AM), or 3D printing, is an innovative technology offering sustainable, customizable, and user-friendly methods across industries. By building products layer by layer, AM significantly reduces material waste and energy consumption, making it an environmentally friendly alternative to traditional manufacturing. Additionally, AM simplifies production with rapid prototyping, digital workflows, and on-demand manufacturing, minimizing costs related to tooling, inventory, and logistics (Javaid et al., 2021), (Bhatia and Sehgal, 2023). This innovative technology allows manufacturers to produce complex structures and multi-material components that were once difficult or impossible to achieve. AM adopts decentralized and localized production, reducing emissions and enabling scalable, cost-efficient processes. Therefore, AM has many applications in different sectors such as manufacturing, aerospace, healthcare, automotive, and construction industry (Ford and Despeisse, 2016).

In the construction sector, AM is particularly well-suited to materials like cement, clay, and concrete, often applied through material extrusion with chemical reaction bonding (MEX-CRB) technology, in which layer-by-layer material deposition results from a chemical reaction facilitating bonding and hardening. Although clay provides sustainability and economy, cementitious materials are extensively used for their strength and durability. Often reinforced or additive-enhanced, concrete offers adaptability for a variety of uses, from structural elements to decorative accents (Khajavi et al., 2021), (Wolf et al., 2022), (Bos et al., 2016).

Geopolymers (GPs), also known as inorganic polymers, have emerged as promising candidates for AM due to their environmental benefits, durability, thermal stability, and resistance to aggressive environments (Raza and Zhong, 2022), (Zaidi et al., 2021), (Lazorenko and Kasprzhitskii, 2022). Synthesized from reactive aluminosilicate sources, such as metakaolin and industrial by-products, GPs form a dense, chemically stable aluminosilicate (N-A-S-H) gel when cured in alkaline conditions, offering superior mechanical and thermal properties compared to conventional materials (Zaidi et al., 2021), (Alghamdi and Neithalath, 2019).

Despite these advantages, GPs have limitations, such as low tensile and flexural strength, which can be mitigated by incorporating fibres like steel, glass, wollastonite or carbon fibres. Acting as crack-bridging elements, fibres delay crack propagation and enhance energy absorption through pull-out mechanisms (Zhang et al., 2025a). Fibre reinforcement improves ductility and crack resistance but increases viscosity, affecting printability (Zaidi et al., 2021), (Ricciotti et al., 2023). Optimizing the raw material composition is essential for tailoring GP properties to specific applications, including underwater construction, where fast-curing, durable materials are required (Korniejenko et al., 2024). In addition, hybrid fibre reinforcement and nano-SiO_2 modification have also been shown to enhance GP performance. Feng et al. (2025) reported improvements in rheology and compressive strength, Zhang et al. (2025b) demonstrated enhanced abrasion resistance through improved fibre–matrix cohesion, Gao et al. (2025) highlighted superior bonding behaviour in repair applications, and Zhang et al. (2025a) reviewed frost resistance mechanisms, emphasizing fibre bridging in crack control.

3D printed GP provides a great degree of freedom, cost and time savings, and low material waste by allowing concrete to be produced from sustainable green materials using a novel building method. The dosage of alkali activator(s), fresh behaviour, and hardened properties depend much on the binder(s) chosen for extrusion-based 3D printing (Jaji et al., 2023a). They exhibit high durability and environmental benefits but have relatively low tensile and flexural strength.

Recent studies have advanced the understanding of GPs for construction, with increasing interest in AM. Ilcan et al. (2023) showed that adjusting alkaline activator content in CDW-based GPs controlled rheology, achieving 65%–82% viscosity recovery and extrudability up to 120 min (except at 15M NaOH). Dai et al. (2024) found that adding 10% metakaolin improved yield stress and strength while reducing CO_2 emissions by ~30%. Gonçalves et al. (2023) demonstrated that polypropylene fibres and optimized printing parameters enhanced the printability and integrity of cylindrical GP samples. Archez et al. (2021) achieved successful printing of hollow cylinders with mineral additives, yielding good layer adhesion, fibre alignment, and flexural strength up to 15 MPa. Jaji et al. (2023b) reported that although slag improved durability, mould-cast specimens outperformed 3D-printed ones in permeability and water absorption, with anisotropic transport observed in printed samples.

Underwater AM applications, such as encapsulating hazardous substances and fabricating artificial reefs, offer innovative solutions for habitat restoration and biodiversity enhancement. AM in underwater environments improves safety, reduces environmental impact, and increases efficiency. While polymers are commonly used, other materials, such as GPs and cement-based mortars, are being extensively studied (Korniejenko et al., 2024). Artificial reefs made with 3D printing can significantly benefit marine habitats, with GPs providing an eco-friendly option, although cement-based mortars like CEM III demonstrate superior durability, biological receptivity, and mechanical efficiency (Yoris-Nobile et al., 2023), (Ly et al., 2021), (Riera et al., 2023).

Some researchers have focused on developing materials suitable for underwater 3D printing. For example, Li et al. (2025) developed anti-washout 3D-printable mortars for underwater construction, showing that silica fume, nano silica, and hydroxypropyl methyl cellulose (HPMC) improved printability and mechanical properties, while glass fibres (GF) had smaller effects. However, combining GF and HPMC caused compatibility issues. Hwalla et al. (2020)

have demonstrated metakaolin-based GPs to be more stable and mechanically retained than cement-based materials for underwater applications. The high viscosity of the alkaline activator improves bonding and underwater placement. GP mixtures outperform cement-based materials underwater with 65%–95% mechanical strength (Hwalla et al., 2020), (Hwalla et al., 2025). Woo et al. (2021) have found that mortars printed underwater had lower density and compressive strength compared to those printed in air, but their interlayer bond strength was slightly higher.

Recent efforts have focused on improving the printability of GPs to support digital construction methods such as 3D printing. However, this often compromises mechanical strength and long-term durability, particularly under conditions like water immersion. For instance, copper slag-based GP blends produced via extrusion have achieved compressive strengths above 40 MPa after 28 days of ambient curing (Kozub et al., 2024). In contrast, binder jet-printed metakaolin-sand GPs showed around 20 MPa strength, with no significant loss after 1 week of water immersion, despite ~30% porosity (Elsayed et al., 2022). Additionally, in precast systems, compressive strength drops sharply during the first 3 days of water immersion but recovers over time, while phase composition remains relatively stable, indicating temporary weakening but structural resilience (Wang et al., 2021). These results highlight the sensitivity of 3D-printed GPs to material formulation, curing, and environmental exposure.

This paper aims to investigate the compressive strength of a metakaolin-based GP reinforced with recycled carbon fibres to enhance its mechanical performance. The research aims to evaluate and compare the mechanical properties of GPs over time in water environments. Samples were produced using three different methods: (i) AM via material extrusion with chemical reaction bonding (MEX-CRB), (ii) extrusion of GP paste underwater using hand force through a syringe, and (iii) conventional casting in moulds in the air. These samples were then submerged in water with varying salt and mineral contents for periods ranging from zero to 3 months. For the syringe-extruded underwater samples, only tap water was used, and the exposure period was extended up to 6 months. The goal is to assess durability, mechanical performance, and environmental impact at defined time intervals. This study suggests that MEX-CRB GPs have lower compressive strength than mould-cast samples due to interlayer and intralayer porosity. However, high-molarity sodium hydroxide could promote rapid setting, and enhance underwater printability and durability. Despite mechanical limits, 3D printing offers benefits like geometric flexibility, material efficiency, and on-site fabrication, making it suitable for specialized infrastructure and repair applications.

2 Materials and methods

To fabricate cubic samples for exposure to different conditions, air, deionized water, fresh lake water, and salt water with the salinity of the Baltic Sea, the GP material composition was prepared. Three different methods were applied in this study: 3D printing by means of MEX-CRB in air, manually printing underwater by syringe, and mould casting in air. In the case of manually printed underwater just one water type, tap water was applied. The aim of this study is to evaluate the compressive strength of GP materials in different environments, compare different manufacturing methods, and analyse the water quality as submarine application of GPs material.

2.1 Preparation of geopolymer

The GP formulation was based on metakaolin with additional reinforcement and functional fillers. The mix consisted of:

1. Metakaolin (MT): Primary aluminosilicate precursor, containing ~52.9% SiO_2 and 41.9% Al_2O_3 with minor oxides (Fe_2O_3 1.1%, TiO_2 1.8%, MgO 0.18%). Particle size distribution: $D_{50} \approx 3$ μm, $D_{90} \approx 10$ μm.
2. Sodium hydroxide solution (NaOH 16 M): Alkaline activator, dissolving aluminosilicates and triggering rapid geopolymerization. Its high alkalinity accelerates metakaolin dissolution, shortens the setting time (90–120 min), and promotes early strength development.
3. Recycled carbon fibres: Sourced from wind farms, with 3 mm length and ~5–7 μm diameter. Bulk density: 0.305 g/cm^3 (Hg porosimetry). Used to reinforce the matrix, enhance compressive/tensile strength, and reduce crack propagation. The 3 mm length was chosen to ensure compatibility with the 4 mm extrusion nozzle.
4. Silica fume (≈96% amorphous SiO_2): Supplementary silicate source, consisting of primary particles (0.1–0.3 μm) and ~30% agglomerates >1 μm. Bulk density: ~200 kg/m^3.
5. Graphite: Very finely ground (~25 μm grain size), with >96% C and <4% ash. Density: ~2.2 g/cm^3. Improves thermal stability, electrical conductivity, and dimensional stability in wet conditions. Recycled graphite from industrial waste also supports circular economy goals and reduces environmental burden (Luo and Wang, 2021).
6. Anhydrite: Calcium-rich additive (industrial gypsum waste) used to control setting time and improve early-age strength. In underwater curing, it may promote secondary C–S–H formation and reduce porosity (Günzel et al., 2024).
7. Alginate: Biopolymer improving the viscosity, workability, and adhesion of the fresh mix.

The combined action of NaOH and anhydrite promotes the formation of a dense N–A–S–H gel, with possible C–A–S–H phases, refining pore structure, lowering permeability, and improving underwater printability and durability.

The mixture has been prepared by considering the following steps: (i) all mixing was performed at room temperature to avoid premature setting due to heat from the reaction, (ii) using mechanical mixing equipment for better consistency, especially when adding carbon fibres and fillers, and (iii) the GP paste may start setting soon after preparation, worked quickly after the final mixing step. Table 1 outlines the composition of the GP mix, highlighting the specific weight fractions of each component for preparing the material.

2.2 Sample preparation

The 3D-Paste Extrusion Development Toolhead (3D-PEDT) piston extruder was used to test small material samples. Due

TABLE 1 Mixture design of the Geopolymer.

Component	MT	NaOH (16M)	CF	Silica	Graphite	Anhydrite	Alginate
Weight fraction (%wt)	0.4706	0.4235	0.0047	0.0470	0.0470	0.0047	0.0023

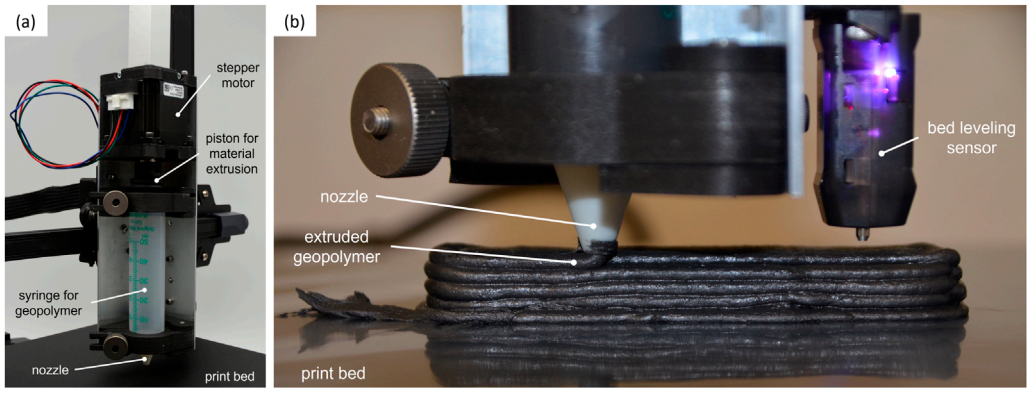

FIGURE 1
(a) Printing setup for MEX-CRB, **(b)** detailed view of the extruding process.

TABLE 2 Printing process parameters for MEX-CRB.

Process parameters	Values
Nozzle diameter [mm]	4
Line width [mm]	5
Layer thickness [mm]	2
Speed [mm/sec]	5
Infill density (%)	100
Infill pattern	concentric

to their simple design and functional similarity, a commercial printer for material extrusion with thermal reaction bonding (MEX-TRB/P) was successfully converted into a MEX-CRB printer. As demonstrated by Denker et al. (2024), a standard 3D desktop printer can be adapted with a paste extrusion system using a commercially available plastic material extruder (MEX-TRB/P), a method applied in this study, as illustrated in Figure 1. Unlike conventional 3D printing methods, this process does not involve any heat source or curing procedure and is carried out at room temperature. Instead, the GP material hardens through a solution-based reaction.

A bar with dimensions 20 × 98 × 20 mm^3 was printed and subsequently, after 14 days of curing, cut into four equal parts, each forming a 20 × 20 × 20 mm^3 cubic sample for compression testing. The printing process parameters are summarized in Table 2.

For manually printed underwater, the moulding frame was submerged in tap water instead of being placed in the air. Using a specialized syringe tube, the material was carefully extruded into the mould to ensure uniform extruding underwater, see Figure 2a. The bars were cut into cubic samples while still in a wet condition, and they remained submerged in water throughout the entire testing period. In this test case, only the exposure of GP materials to tap water will be examined, as they were manufactured directly underwater.

For mould casting in air, bar samples were first fabricated using a moulding process in air and then cut into cubic samples. A moulding frame was prepared to create bars with dimensions of 20 × 160 × 20 mm^3. The material was poured into the moulds, and after 14 days of curing, the samples were cut into cubic forms and prepared for long-term experiments in various environments. Figure 2b shows the GP materials after moulding into bar-shaped forms.

2.3 Testing of mechanical properties

The compressive strength test was carried out in accordance with ISO 1920–4:2020–01, which specifies three samples in minimum for determining the compressive strength. The cubic samples were tested on a universal testing machine model MTS 880 with a 100 kN measuring cell. A load speed of 6 mm/min was used and four specimens were tested per environment condition and time interval.

To investigate the behaviour of GP in mould-cast and 3D-printed samples under different environmental conditions, samples were placed in four different environments air, deionized-, lake- and salt water with the salinity of the Baltic Sea for varying time intervals (baseline, 1 month, and 3 months). The compressive force was applied perpendicular to the layer buildup direction in 3D-printed samples and to the free surface of the mould-cast specimens. A summary of experimental conditions, testing, and specimen details is illustrated in Table 3.

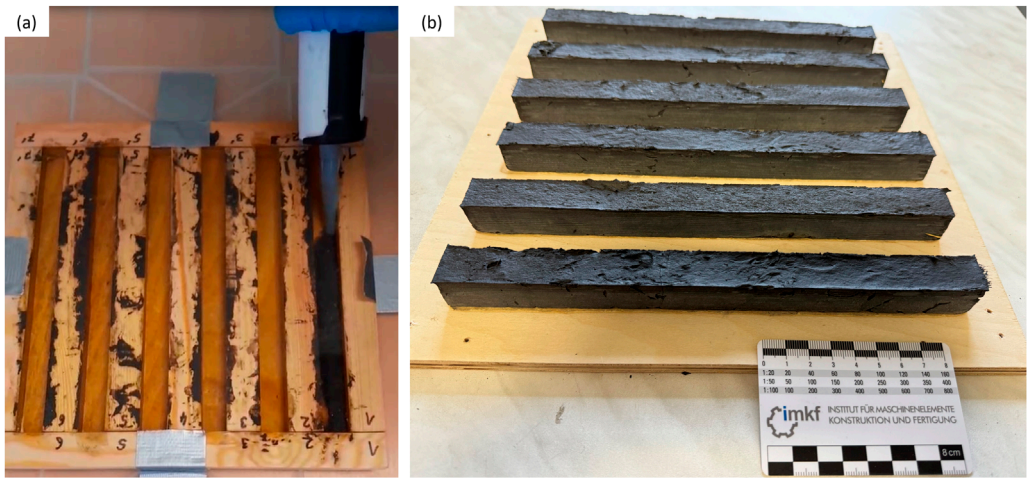

FIGURE 2
(a) Geopolymer printed in tab water and **(b)** casted in air after demoulding.

TABLE 3 Summary of experimental conditions, testing, and specimen details.

Manufacturing type	Environmental cure conditions	Storage condition	Age at testing	No. of specimens	Test standard	Specimen dimensions
MEX-CRB (Printed in Air)	14 days in air	air deionized water lake water salt water	0 days 1 month, 3 months	4 per interval	ISO 1920–4:2020–01	20 × 20 × 20 mm^3
Manually Printed Underwater	extruded and cured directly in water	tap water	0 days 2 weeks 4 weeks 6 weeks, 12 weeks 24 weeks	4 per interval	ISO 1920–4:2020–01	20 × 20 × 20 mm^3
Mould-Cast (in Air)	14 days in air	air deionized water, lake water salt water	0 days 1 month 3 months	4 per interval	ISO 1920–4:2020–01	20 × 20 × 20 mm^3

3 Results and discussion

3.1 Compressive strength

The baseline, day zero, condition applies only to air-exposed samples manufactured by mould-casting and MEX-CRB to determine their initial compressive strength at the start of the long-term experiment. Subsequently, compressive tests were conducted on both sample types after one and 3 months in different environments. Figure 3 illustrates the compressive strength of these samples. The results reveal that mould-cast samples in air exhibit the highest compressive strength, reaching approximately 50 MPa, whereas 3D-printed samples in air demonstrate significantly lower strength, around 20 MPa, see Figure 3.

When exposed to water environments, such as deionized, lake or salt water, the compressive strength of all samples generally decreases. However, mould-cast samples consistently retain higher strength and force values compared to 3D-printed samples across all conditions. The most noticeable strength degradation occurs in water-immersed conditions, where both sample types show reduced values over time. A consistent trend emerges, demonstrating that mould-cast samples outperform 3D-printed samples in all environments. The largest strength difference is observed in air, but this gap narrows slightly in water-exposed conditions. For instance, after 3 months in salt water, mould-cast samples still exhibit strengths around 30 MPa, whereas 3D-printed samples remain slightly below 20 MPa.

These findings indicate that mould-casting offers higher mechanical performance compared to 3D printing, particularly in dry conditions. However, exposure to water further weakens both sample types, though mould-cast samples consistently retain relatively higher strength and require greater force for failure. The box chart overlays and error bars highlight variability within the dataset, suggesting possible inconsistencies arising from both

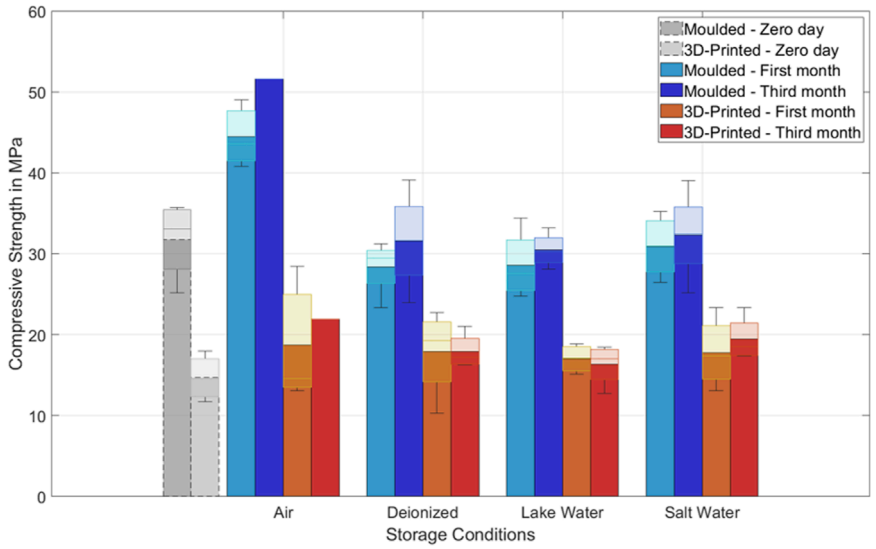

FIGURE 3
Compressive strength for different storage conditions to compare mould-cast and 3D printed samples.

material-related factors and experimental conditions, such as voids from mould casting or weak interlayer bonding in 3D-printed specimens, that may influence the final compressive strength and force measurements.

Dimensional and physical changes were assessed by comparing baseline and pre-test values after water exposure. Figure 4 presents the mean percentage differences in mass (top left), density (top right), width (bottom left), and height (bottom right) for mould-cast and 3D-printed samples after exposure to deionized, lake, and salt water for one and 3 months.

Mass changes (Figure 4a) reveal that all specimens absorbed water, with moulded samples showing moderate increases (~5–6%) and 3D-printed ones higher gains (~8–11%). In salt water, the samples show the highest mass absorption because of both water and salt. Density variations (Figure 4b) were between 10% and 15% for all groups. Both mould-cast and 3D-printed samples showed a similar trend, with only minor changes during exposure, indicating that water environment had limited influence on density. Dimensional changes were minor compared to mass and density. Width (Figure 4c) remained nearly constant across all environments; in 3D-printed and moulded specimens, almost all values were slightly negative and close to zero. Height changes (Figure 4d), however, showed a clear contrast: mould-cast specimens contracted markedly, approaching several percent shrinkage (~3–8%), whereas 3D-printed samples fluctuated between minor shrinkage and swelling within about ±1%–2%, remaining overall closer to dimensional stability. In summary, mould-cast samples demonstrated lower water uptake but greater shrinkage, while 3D-printed samples absorbed more water yet retained better geometric stability.

Moreover, the compressive strength of the hand-printed samples underwater has been examined over different time intervals (zero, two, four, six, twelve and 24 weeks). Figure 5 presents the result of the compressive tests over different time intervals. The samples were removed from the water 1 hour before the test, measured, and stored in an airtight bag.

Observing the trends, the strength increases from the Baseline, day zero from ~8 MPa to the second week to ~13 MPa, suggesting material hardening or improved curing over time also underwater. The highest compressive strength occurs on the fourth week with ~14–15 MPa, but with high variability, as indicated by the larger boxplot and extended error bars. By the sixth week and 12th week, the strength stabilizes by ~13 MPa, with reduced variation, as seen in the smaller box and shorter error bars. By week 24, a slight decrease in strength is observed, with values dropping to ~11.5 MPa, indicating a potential plateau or mild degradation in mechanical performance over extended immersion. These results confirm that these samples experience ongoing strength development underwater, with curing effects enhancing performance up to a point. The fourth week marks the peak strength phase, while subsequent weeks show stabilization or modest decline, suggesting a limit to underwater curing benefits over time.

The compressive strength of our 3D-printed samples (approximately 20 MPa in air, lower in water) falls within the lower range reported for printable GP systems (Elsayed et al., 2022), and remains well below values achieved in optimized mixes incorporating copper slag or improved curing protocols, which exceed 40 MPa (Kozub et al., 2024). This supports the common observation that enhancing printability, through reduced solid content or adjusted rheology, can compromise mechanical performance, particularly under challenging conditions such as water immersion (Wang et al., 2021).

Figure 6 shows two microscope images at ×20 magnification of the cast, additively manufactured, and manually syringe-printed cubic samples in water before and after the compression test. The 3 mm long recycled carbon fibres in the printed samples are unidirectionally aligned in the printing direction, whereas the carbon fibres in the cast samples are non-directional. Regardless of

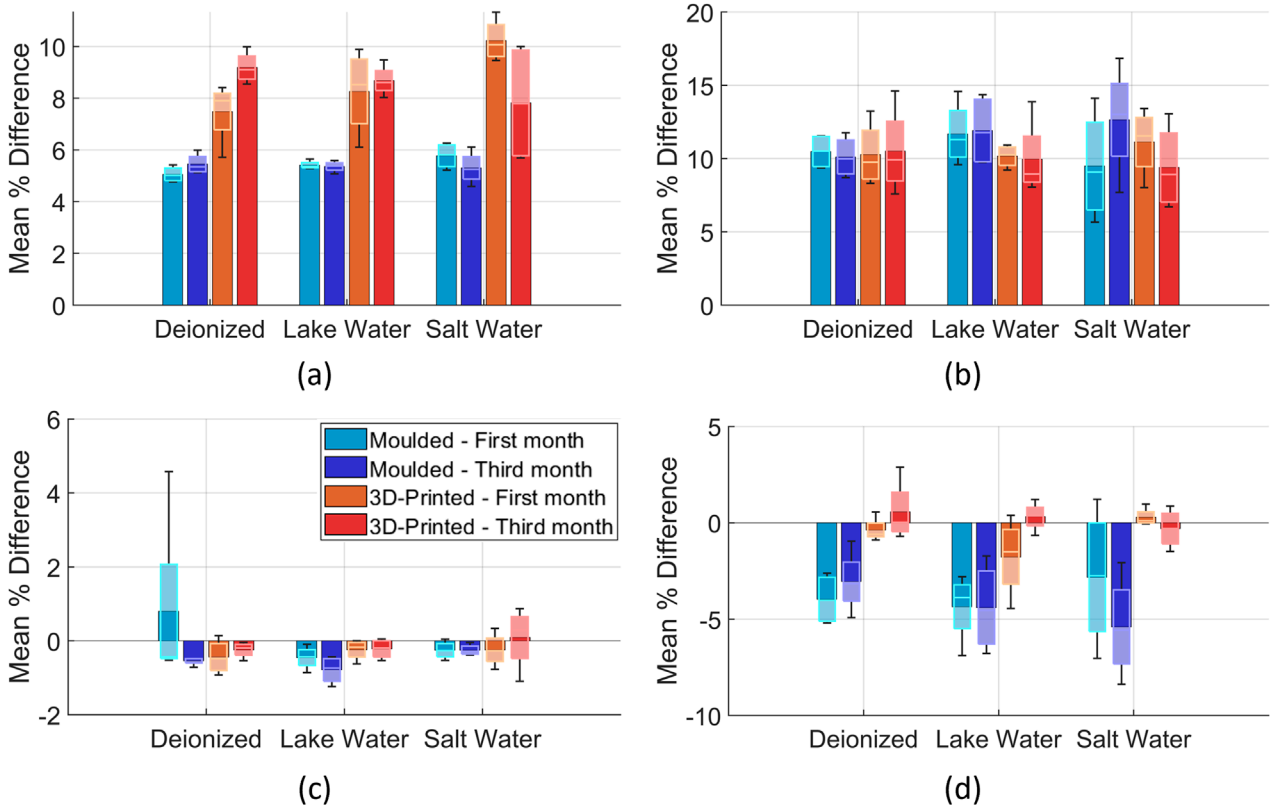

FIGURE 4
Physical and dimensional changes of the test specimens after water exposure: **(a)** mass, **(b)** density, **(c)** width, and **(d)** height.

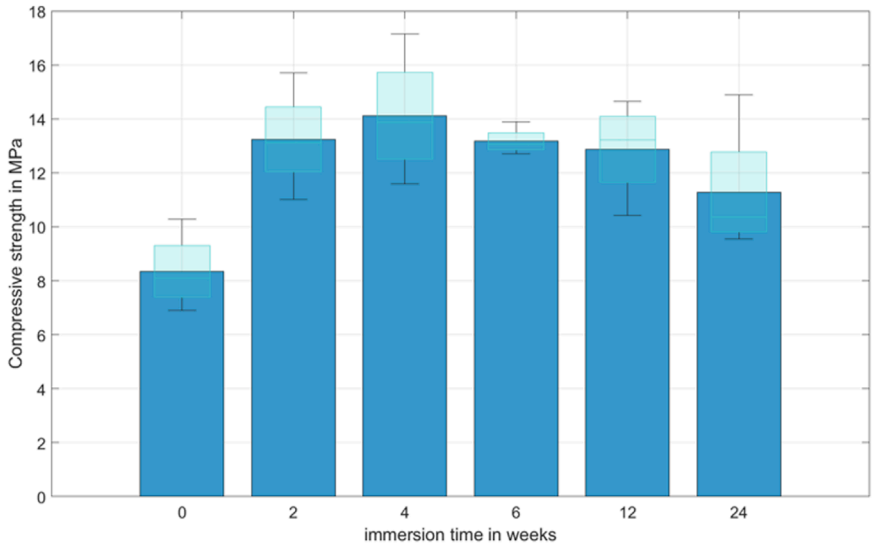

FIGURE 5
Compressive strength up to 3 months for manually printed by syringe underwater.

the manufacturing process, almost all samples have pores on the analysed cut surfaces.

The size of the pores also varied from microscopic to macroscopic with up to 4 mm. The pores and defects of the moulded samples are mostly roundish and occasionally oval with vertical orientation, Figure 6a, whereas the pores of the samples processed with MEX-CRB and the syringe samples are mostly elongated in the direction of printing, round pores are hardly pronounced, Figure 6b.

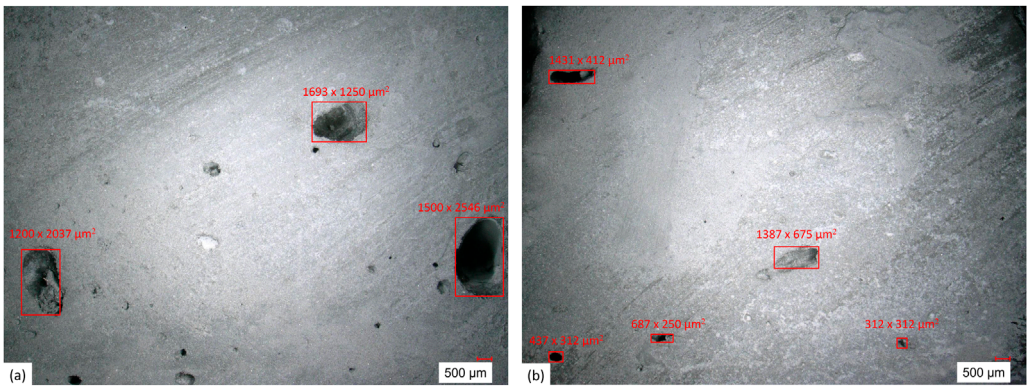

FIGURE 6
Microscope image, 20x magnification, comparison of the pores of **(a)** moulded and **(b)** printed samples before compression test.

Elongated, oval pores have a larger surface area than round pores, which also provides a larger reaction surface for the GP with water. This may be the reason for the reduced compressive strength of the printed GP.

Regardless of the manufacturing process, all samples exhibited brittle fracture behaviour. Only the samples printed manually with a syringe in water initially deformed into a trapezoidal shape after 2 weeks of storage in water before the brittle fracture occurred. In addition, the residual moisture was pressed out of the specimen. The curing process of the GP was not yet complete at this point. The compressive strength tests show that the final strength of the GP is reached after 28 days, as with conventional concretes. At the end of the 28 days, brittle fracture occurred in all samples without further deformation.

The brittle fracture of the cast samples always occurred parallel to the direction of force application. Occasionally, small, thin material flaking occurred on the sides of the samples. Figure 7 shows the brittle fracture on the left, in the upper area pores and the non-directional carbon fibres can be seen, which are visible through the material spalling.

In the samples produced with MEX-CRB, in addition to the brittle fractures running parallel to the force application, Figure 8a, there are also cracks between the layers, Figure 8b. The areas between the deposited pressure paths behave like notches; in contrast to casting, the material properties of the GP are not homogeneous in this area, which favours fracture. Due to the additive manufacturing process, there are more pore accumulations between the deposited webs in this area, which further favours the fracture effect.

The effect of cracks in the print paths is less pronounced with samples printed manually with a syringe in water than with MEX-CRB, as the material immediately comes into contact with water when it emerges from the syringe. The toughness of the GP decreases and cavities and unevenness in the deposited print paths are levelled out, reducing the accumulation of pores.

CF improve fracture behaviour through crack bridging and pull-out, delaying crack propagation and absorbing energy. In mould-cast samples, randomly oriented fibres provide multidirectional reinforcement and higher strength, whereas in printed samples, fibre alignment and interlayer weaknesses limit stress transfer and reduce load capacity (Figure 8a).

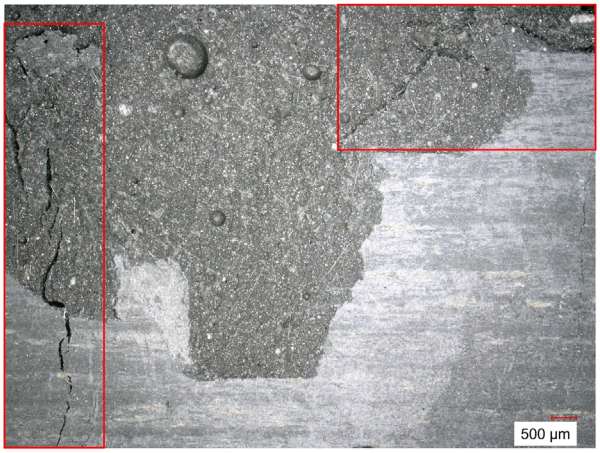

FIGURE 7
Microscope image, 30x magnification, flaking and fracture pattern of the sample moulded in air after compression test.

Figure 9 shows the representative force–displacement responses of mould-cast and printed samples stored in different environments, corresponding to the compressive strength results presented in Figure 3. For clarity, only one specimen per storage condition and manufacturing route is displayed. The curves indicate higher peak forces and more stable post-peak behaviour for mould-cast samples, while printed samples show lower load capacity and steeper softening. The jagged shape of many curves, characterized by sudden load drops followed by recovery, reflects fibre debonding, pull-out, matrix heterogeneity, and interlayer weaknesses for printed samples.

It is worth noticing that the behaviour of CF in the GP matrix is coherent with previous research; they enhance the mechanical properties of the material (Růžek et al., 2023), (Hassan et al., 2025). However, the comparative works on the usage of the AM technology usually show better properties obtained in the case of the casted materials (Korniejenko et al., 2022). It should be noted that in the case of 3D printed elements, this kind of reinforcement can play an

10.3389/fbuil.2025.1620385

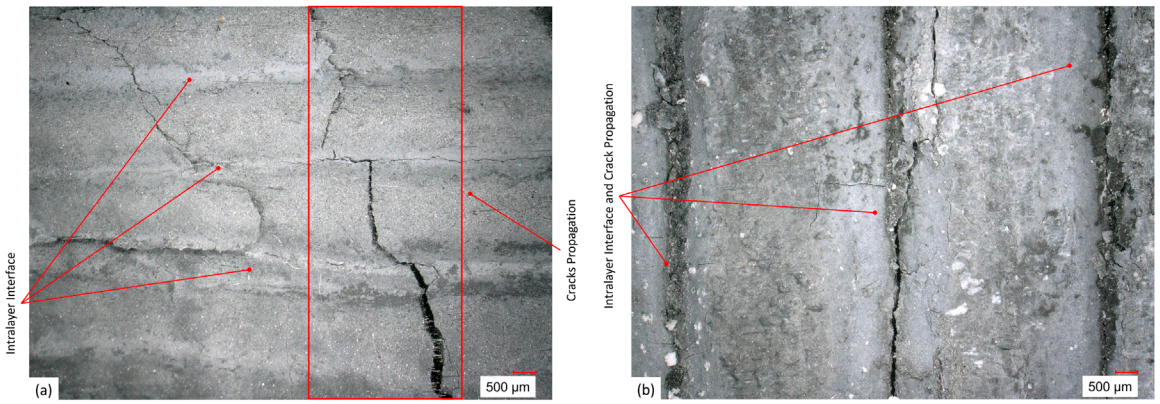

FIGURE 8
Microscope image, 30x magnification, fracture behaviour of specimens produced with MEX-CRB, **(a)** fracture parallel to force direction and perpendicular to layer interfaces, illustrating carbon fibres aligned along the extrusion path inside the crack and **(b)** crack propagation parallel to layer interfaces and within the printed layers.

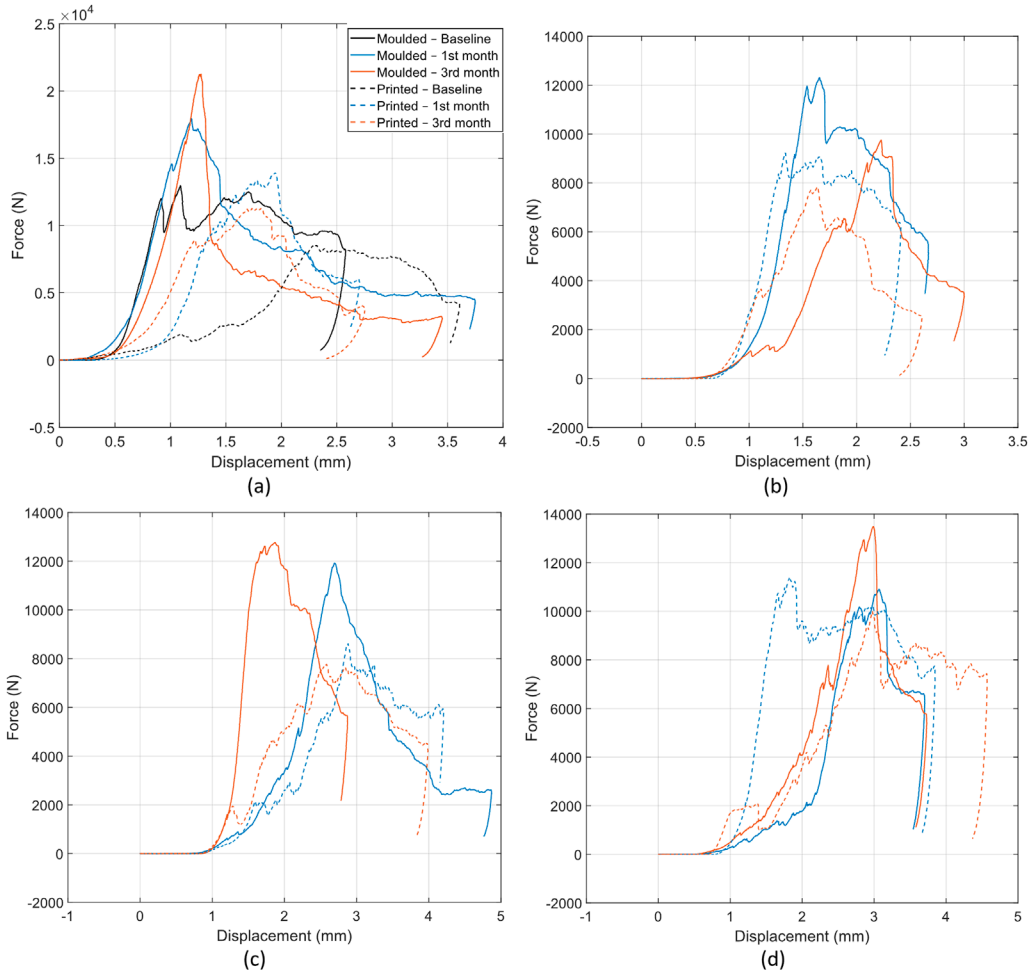

FIGURE 9
Force–displacement responses of geopolymer specimens in **(a)** air, **(b)** deionized water, **(c)** lake water, and **(d)** salt water. Curves are shown for mould-cast and 3D-printed samples at baseline (air only), after 1 month, and after 3 months of storage.

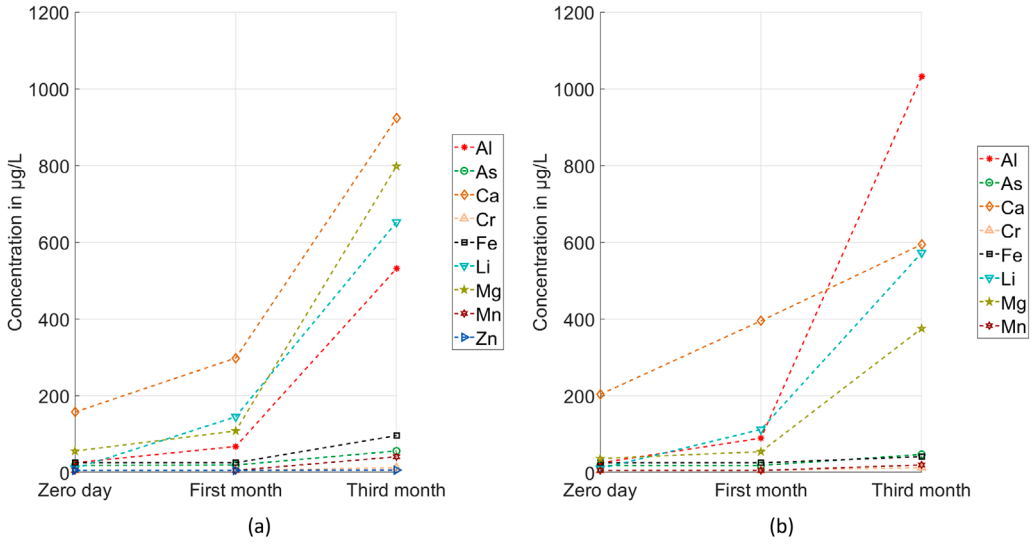

FIGURE 10
Water analysis from deionized water at day zero and after one and 3 months, **(a)** MEX-CRB and **(b)** moulded.

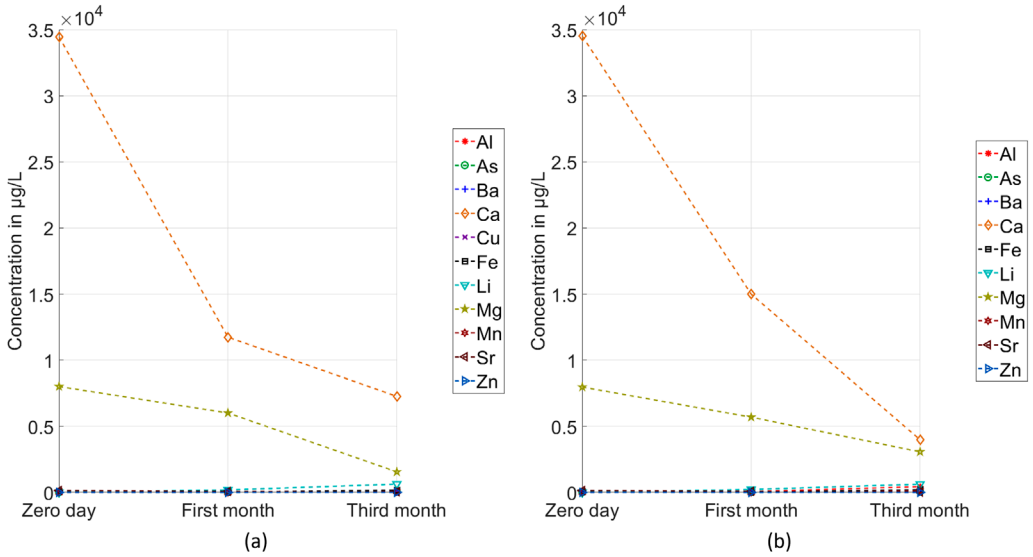

FIGURE 11
Water analysis from lake water at day zero and after one and 3 months, **(a)** MEX-CRB and **(b)** moulded.

even more important function. In the case of using AM, there are limited possibilities to implement other forms of reinforcement into the composition. Traditional bars are completely not coherent with this technology and the possibility of implementation of continuous reinforcement is also limited (Lv et al., 2022). In this case, the short fibres are the only reasonable option. This kind of reinforcement has to be carefully selected according 3D printing parameter process to obtain proper cohesion between fibre and matrix material. With the above limitations, it should also be taken into account that the 3D printing process itself will affect the mechanical properties of the material; in particular, it will be characterised by significant changes in properties depending on the direction of research (Lv et al., 2022), (Maralapalle et al., 2025). An additional limitation is that the usage of recycled fibres is a kind of compromise between improving the material properties and reducing the environmental impact of the material. Current recycling technologies significantly influence the final properties of the CF, lowering their properties compared to virgin ones (Růžek et al., 2023), (Yu et al., 2025).

3.2 Water analysis

In order to investigate the long-term interaction of GP composites with recycled carbon fibres under realistic and

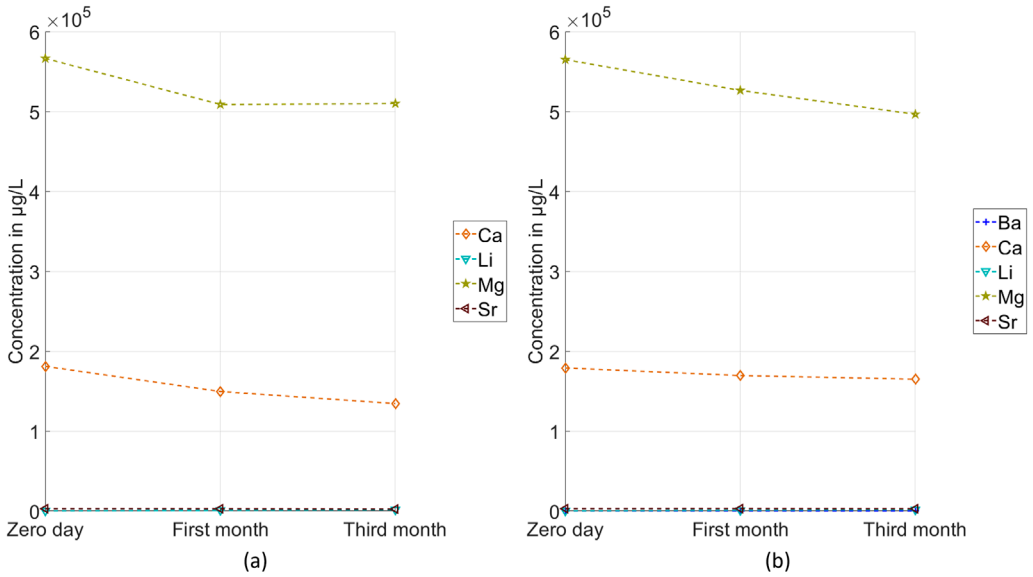

FIGURE 12
Water analysis from salt water at day zero and after one and 3 months, **(a)** MEX-CRB and **(b)** moulded.

chemically diverse aquatic conditions, samples produced via both casting and AM were immersed in three different water types: deionized water, synthetic seawater (simulating Baltic Sea salinity), and untreated lake water. The water quality development over a period of 3 months was assessed in terms of ionic conductivity and visible changes in water and sample surfaces. The presence of metals in the water was analysed using ion chromatography with the 850 Professional IC measuring device from Metrohm.

The selection of these three water types serves to simulate a range of realistic environmental and laboratory conditions. Deionized water, while not distilled, was obtained from a workshop filtration system and is intended to provide a controlled, low-ion background to observe the baseline leaching behaviour of ions from the GP materials. Synthetic seawater was created by dissolving 200 g of marine-grade salt in 10 L of deionized water and was used to replicate the alkaline and saline conditions similar to those of the Baltic Sea. This setup aims to determine whether the presence of salts and elevated ionic strength changes the leaching behaviour or affects the structural stability of the composites. Untreated lake water, containing natural microorganisms and organic matter, introduces a biologically active environment, enabling investigation into potential biofilm formation, biological degradation or surface colonization effects. All samples - both printed and cast - were placed in water containers after production. By combining both manufacturing techniques with the three distinct water types, a total of six experimental containers were prepared. Each container held a volume of 10 L and was stored at room temperature in a location protected from direct sunlight to avoid temperature fluctuations or biological bias. This experimental design enables a comprehensive investigation of the durability of the GP composites under various long-term exposure conditions.

The analysis of the element concentrations in deionized water, Figure 10, over time reveals a continuous increase for both printed and moulded samples, indicating that substances are consistently leaching from the GP composites into the surrounding water. This suggests that the materials are not chemically inert under these conditions and actively release elements into the solution.

At the beginning of the experiment, all measured elements - except for calcium and magnesium - were very low and partly below the detection limit. The measured elements, calcium, magnesium, lithium, and aluminium show the most significant increases in concentration. These elements likely originate from the GP matrix or residual phases associated with the recycled carbon fibres. Their increased presence points to either partial dissolution of specific mineral phases or ongoing ion exchange processes at the material-water interface (e.g., metakaolin and anhydrites).

Both types of samples - printed and moulded - show similar leaching behaviour over the observed period, indicating comparable material-water interactions. However, it is noteworthy that the aluminium concentration in the cast specimen shows a distinctly stronger increase after 3 months compared to the printed variant. The concentrations for calcium, magnesium, and lithium increase less in the container with the moulded samples.

Importantly, the fact that concentrations have not plateaued by the end of the three-month observation period implies that chemical equilibrium has not yet been reached in either system. This indicates the potential for continued leaching over longer timeframes. Especially in large bodies of water, there will always be dilution in contrast to the buckets used.

In the lake water, Figure 11a, calcium and magnesium concentrations were initially high, reflecting the natural composition of the freshwater environment. Unlike in deionized water, these concentrations decreased over time, indicating potential precipitation of these ions or uptake by biological activity such as algae or biofilms forming on the sample surfaces.

The behaviour of the other measured elements was comparable to that observed in the deionized water experiments. This suggests

that, aside from the calcium and magnesium concentrations, the leaching behaviour of the GP materials is consistent across both water types.

As seen previously, the aluminium concentration in the moulded samples was again higher after 3 months than in the printed ones. This aligns with the observations in deionized water and supports the assumption that the casting process might favour the release of aluminium due to differences in the material structure.

In the saline water environment, Figure 12, only a limited number of elements could be reliably quantified. Due to the salt content, the samples had to be diluted before being analysed as the concentration exceeded the measuring range of 0.5–200 mg/L. This resulted in some metal concentrations falling below the detection limits of the measuring devices. As a result, fewer elements were measurable compared to the deionized and lake water conditions.

Notably, the concentrations of several detected elements decreased over time. This behaviour is consistent with the visual observation of white precipitates forming on the surfaces of the samples, indicating the removal of certain ions from the water column via precipitation. Furthermore, all other elements remained at significantly lower concentrations.

4 Conclusion

This study demonstrates the potential of additively manufactured GPs, particularly for underwater applications such as the stabilization of environmentally hazardous structures like shipwrecks. The ability to replicate complex geometries and create bio-receptive surfaces supports their use in ecological restoration and marine infrastructure.

While the results confirm the environmental advantages and feasibility of additive manufacturing with GPs, several limitations were identified. In particular, 3D-printed samples exhibited lower compressive strength compared to mould-cast ones, primarily due to interlayer porosity and weak bonding. However, the use of high-molarity alkaline activators contributed to satisfactory underwater curing and dimensional stability over time.

Water analysis revealed ongoing leaching behaviour in all specimens, emphasizing the need for further investigation into long-term chemical stability. Observed microstructural differences between manufacturing methods also indicate that processing technique significantly influences pore morphology and, consequently, mechanical performance.

Overall, the findings support the viability of 3D-printed GPs for specialized underwater applications but highlight the importance of continued research into durability, mechanical performance, and environmental compatibility.

Future work stemming from this study can be continued by considering the following directions:

1. Extended Durability Studies: A three-month exposure period is insufficient to evaluate long-term performance. Future studies should include extended timeframes of 6 months to 1 year to better assess durability and leaching behaviour.
2. Mixture Optimization: Investigate alternative mix designs, including formulations without fibres or using virgin carbon fibres, to balance printability and strength.
3. Mechanical Behaviour: Explore flexural and tensile strength, fracture toughness, and fatigue resistance under aquatic conditions to complement compressive strength data.
4. Curing Strategies: Develop environmentally friendly methods to accelerate the curing process and reduce both early-stage and long-term leaching, enabling more complex geometries and faster implementation in marine environments.

Data availability statement

The raw data supporting the conclusions of this article will be made available by the authors, without undue reservation.

Author contributions

MD: Writing – original draft, Writing – review and editing. BG: Writing – review and editing, Writing – original draft. RG: Writing – review and editing, Writing – original draft. SP: Writing – review and editing. KK: Writing – review and editing. TG: Writing – review and editing. HZ: Writing – review and editing.

Funding

The author(s) declare that financial support was received for the research and/or publication of this article. The project MAR-Wreck is co-financed with tax funds on the basis of the budget passed by the Saxon State Parliament (SAB) and is supported by the European network M-ERA.NET 3 program by the grant number M-ERA.NET3/2021/71/MAR-WRECK/2022.

Conflict of interest

The authors declare that the research was conducted in the absence of any commercial or financial relationships that could be construed as a potential conflict of interest.

The author(s) declared that they were an editorial board member of Frontiers, at the time of submission. This had no impact on the peer review process and the final decision.

Generative AI statement

The author(s) declare that no Generative AI was used in the creation of this manuscript.

Any alternative text (alt text) provided alongside figures in this article has been generated by Frontiers with the support of artificial intelligence and reasonable efforts have been made to ensure accuracy, including review by the authors wherever possible. If you identify any issues, please contact us.

Publisher's note

All claims expressed in this article are solely those of the authors and do not necessarily represent those of their affiliated

organizations, or those of the publisher, the editors and the reviewers. Any product that may be evaluated in this article, or claim that may be made by its manufacturer, is not guaranteed or endorsed by the publisher.

References

Alghamdi, H., and Neithalath, N. (2019). Synthesis and characterization of 3D-printable geopolymeric foams for thermally efficient building envelope materials. *Cem. Concr. Compos* 104, 103377. doi:10.1016/j.cemconcomp.2019.103377

Archez, J., Texier-Mandoki, N., Bourbon, X., Caron, J. F., and Rossignol, S. (2021). Shaping of geopolymer composites by 3D printing. *J. Build. Eng.* 34, 101894. doi:10.1016/j.jobe.2020.101894

Bhatia, A., and Sehgal, A. K. (2023). Additive manufacturing materials, methods and applications: a review. *Mater Today Proc.* 81, 1060–1067. doi:10.1016/j.matpr.2021.04.379

Bos, F., Wolfs, R., Ahmed, Z., and Salet, T. (2016). Additive manufacturing of concrete in construction: potentials and challenges of 3D concrete printing. *Virtual Phys. Prototyp.* 11 (3), 209–225. doi:10.1080/17452759.2016.1209867

Dai, X., Tao, Y., Zhang, Y., Ding, L., Van Tittelboom, K., and De Schutter, G. (2024). Development of 3D printable alkali-activated slag-metakaolin concrete. *Constr. Build. Mater* 444, 137775. doi:10.1016/j.conbuildmat.2024.137775

Denker, M., Lamottke, M., Kühnel, L., Micke, L., and Zeidler, H. (2024). "Material extrusion printer for pastes based on a commercial desktop filament printer for plastics," in *1st open source hardware konferenz 2024*. doi:10.69558/2024004

Elsayed, H., Gobbin, F., Picicco, M., Italiano, A., and Colombo, P. (2022). Additive manufacturing of inorganic components using a geopolymer and binder jetting. *Addit. Manuf.* 56 (Aug), 102909. doi:10.1016/j.addma.2022.102909

Feng, Z., Zhang, P., Guo, J., Zheng, Y., and Hu, S. (2025). Single and synergistic effects of nano-SiO2 and hybrid fiber on rheological property and compressive strength of geopolymer concrete. *Constr. Build. Mater* 472 (Apr), 140945. doi:10.1016/j.conbuildmat.2025.140945

Ford, S., and Despeisse, M. (2016). Additive manufacturing and sustainability: an exploratory study of the advantages and challenges. *J. Clean. Prod.* 137, 1573–1587. doi:10.1016/j.jclepro.2016.04.150

Gao, Z., Zhang, P., Dai, X., Zheng, Y., and Feng, H. (2025). Assessment of bonding behavior of hybrid fiber alkali-activated concrete for tunnel lining concrete restoration. *J. Clean. Prod.* 514 (Jul), 145803. doi:10.1016/j.jclepro.2025.145803

Gonçalves, C. E. C., Ribeiro, T. M., and Santos, S. F. (2023). 3D printing using metakaolin-based geopolymers - challenges. *Ceramica* 69 (392), 340–345. doi:10.1590/0366-69132024703923508

Günzel, F. S., Moelich, G. M., Kanyenze, S. S., Kruger, P. J., and Combrinck, R. (2024). Investigating inherent cement setting mechanisms to improve the constructability performance of extrusion-based 3D concrete printing. *Innov. Infrastruct. Solutions* 9 (12), 480. doi:10.1007/s41062-024-01788-9

Hassan, A., Alomayri, T., Noaman, M. F., and Zhang, C. (2025). 3D printed concrete for sustainable construction: a review of mechanical properties and environmental impact. *Arch. Comput. Methods Eng.* 32, 2713–2743. doi:10.1007/s11831-024-10220-5

Hwalla, J., Saba, M., and Assaad, J. J. (2020). Suitability of metakaolin-based geopolymers for underwater applications. *Mater Struct.* 53 (5), 119. doi:10.1617/s11527-020-01546-0

Hwalla, J., Saba, M., and El-Hachem, H. (2025). "Performance of metakaolin-based alkali-activated mortar for underwater placement," in The 1st international conference on net-zero built environment. Editors M. Kioumarsi, and B. Shafei (Cham: Springer Nature Switzerland), 93–104.

Ilcan, H., Sahin, O., Kul, A., Ozcelikci, E., and Sahmaran, M. (2023). Rheological property and extrudability performance assessment of construction and demolition waste-based geopolymer mortars with varied testing protocols. *Cem. Concr. Compos* 136, 104891. doi:10.1016/j.cemconcomp.2022.104891

Jaji, M. B., van Zijl, GPAG, and Babafemi, A. J. (2023a). Slag-modified metakaolin-based geopolymer for 3D concrete printing application: evaluating fresh and hardened properties. *Clean. Eng. Technol.* 15, 100665. doi:10.1016/j.clet.2023.100665

Jaji, M. B., Ibrahim, K. A., van Zijl, GPAG, and Babafemi, A. J. (2023b). Effect of anisotropy on permeability index and water absorption of 3D printed metakaolin-based geopolymer concrete. *Mater Today Proc.* 84, 1000–1007. doi:10.1016/j.matpr.2023.06.394

Javaid, M., Haleem, A., Singh, R. P., Suman, R., and Rab, S. (2021). Role of additive manufacturing applications towards environmental sustainability. *Adv. Ind. Eng. Polym. Res.* 4 (4), 312–322. doi:10.1016/j.aiepr.2021.07.005

Khajavi, S. H., Tetik, M., Mohite, A., Li, A., Peltokorpi, M., Weng, Y., et al. (2021). Additive manufacturing in the construction industry: the comparative competitiveness of 3D concrete printing. *Appl. Sci.* 11 (9), 3865. doi:10.3390/app11093865

Korniejenko, K., Kejzlar, P., and Louda, P. (2022). The influence of the material structure on the mechanical properties of geopolymer composites reinforced with short fibers obtained with additive technologies. *Int. J. Mol. Sci.* 23, 2023. doi:10.3390/ijms23042023

Korniejenko, K., Gądek, S., Dynowski, P., Tran, D. H., Rudziewicz, M., Pose, S., et al. (2024). Additive manufacturing in underwater applications. *Appl. Sci.* 14 (4), 1346. doi:10.3390/app14041346

Kozub, B., Sitarz, M., Gądek, S., Ziejewska, C., Mróz, K., and Hager, I. (2024). Upscaling of copper slag-based geopolymer to 3D printing technology. *Materials* 17 (22), 5581. doi:10.3390/ma17225581

Lazorenko, G., and Kasprzhitskii, A. (2022). Geopolymer additive manufacturing: a review. *Addit. Manuf.* 55, 102782. doi:10.1016/j.addma.2022.102782

Li, L. G., Zhang, G. H., and Kwan, A. K. H. (2025). Exploring submarine 3D printing: enhancing washout resistance and strength of 3D printable mortar. *J. Mater Civ. Eng.* 37 (3), 04025019. doi:10.1061/JMCEE7.MTENG-19089

Luo, T., and Wang, Q. (2021). Effects of graphite on electrically conductive cementitious composite properties: a review. *Materials* 14 (17), 4798. doi:10.3390/ma14174798

Lv, C., Shen, H., Liu, J., Wu, D., Qu, E., and Liu, S. (2022). Properties of 3D printing fiber-reinforced geopolymers based on interlayer bonding and anisotropy. *Materials* 15, 8032. doi:10.3390/ma15228032

Ly, O., Yoris-Nobile, A. I., Sebaibi, N., Blanco-Fernandez, E., Boutouil, M., Castro-Fresno, D., et al. (2021). Optimisation of 3D printed concrete for artificial reefs: biofouling and mechanical analysis. *Constr. Build. Mater* 272, 121649. doi:10.1016/j.conbuildmat.2020.121649

Maralapalle, V., Kumavat, H. R., Nadaf, M. B., Zende, A. A., Mishra, S. S., and Iyer, R. (2025). Optimizing 3D geopolymer concrete for sustainable construction: a review of material selection, printing methods, and properties. *Innov. Infrastruct. Solut.* 10, 174. doi:10.1007/s41062-025-01970-7

Raza, M. H., and Zhong, R. Y. (2022). A sustainable roadmap for additive manufacturing using geopolymers in construction industry. *Resour. Conserv. Recycl* 186, 106592. doi:10.1016/j.resconrec.2022.106592

Ricciotti, L., Apicella, A., Perrotta, V., and Aversa, R. (2023). Geopolymer materials for extrusion-based 3D-Printing: a review. *Polym. (Basel)* 15 (24), 4688. doi:10.3390/polym15244688

Riera, E., Hubas, C., Ungermann, M., Rigot, G., Pey, A., Francour, P., et al. (2023). Artificial reef effectiveness changes among types as revealed by underwater hyperspectral imagery. *Restor. Ecol.* 31 (8), e13978. doi:10.1111/rec.13978

Růžek, V., Dostayeva, A. M., Walter, J., Grab, T., and Korniejenko, K. (2023). Carbon fiber-reinforced geopolymer composites: a review. *Fibers* 11, 17. doi:10.3390/fib11020017

Wang, S., Yu, L., Xu, L., Wu, K., and Yang, Z. (2021). The failure mechanisms of precast geopolymer after water immersion. *Materials* 14 (18), 5299. doi:10.3390/ma14185299

Wolf, A., Rosendahl, P. L., and Knaack, U. (2022). Additive manufacturing of clay and ceramic building components. *Autom. Constr.* 133, 103956. doi:10.1016/j.autcon.2021.103956

Woo, S. J., Yang, J. M., Lee, H., and Kwon, H. K. (2021). Comparison of properties of 3D-Printed mortar in air vs. underwater. *Materials* 14 (19), 5888. doi:10.3390/ma14195888

Yoris-Nobile, A. I., Slebi-Acevedo, C. J., Lizasoain-Arteaga, E., Indacoechea-Vega, I., Blanco-Fernandez, E., Castro-Fresno, D., et al. (2023). Artificial reefs built by 3D printing: systematisation in the design, material selection and fabrication. *Constr. Build. Mater* 362, 129766. doi:10.1016/j.conbuildmat.2022.129766

Yu, X., Zhang, C., Li, J., Bai, X., Yang, L., Han, J., et al. (2025). Reuse of retired wind turbine blades in civil engineering. *Buildings* 15, 2414. doi:10.3390/buildings15142414

Zaidi, F. H. A., Ahmad, R., Abdullah, M. M. A., Abd Rahim, S. Z., Yahya, Z., Li, L. Y., et al. (2021). Geopolymer as underwater concreting material: a review. *Constr. Build. Mater* 291, 123276. doi:10.1016/j.conbuildmat.2021.123276

Zhang, P., Wen, Z., Han, X., Guo, J., and Hu, S. (2025a). *A state-of-the-art review on frost resistance of fiber-reinforced geopolymer composites*. Elsevier B.V. doi:10.1016/j.scp.2025.102006

Zhang, P., Wang, W., Guo, J., and Zheng, Y. (2025b). Abrasion resistance and damage mechanism of hybrid fiber-reinforced geopolymer concrete containing nano-SiO2. *J. Clean. Prod.* 494 (Feb), 144971. doi:10.1016/j.jclepro.2025.144971